Int. J. Engng Sci. Vol. 25, No. 9, pp. 1131–1141, 1987
Printed in Great Britain. 
0020-7225/87 $3.00 + 0.00


# STEADY-STATE PENETRATION OF VISCOPLASTIC TARGETS

R. C. BATRA
Department of Engineering Mechanics, University of Missouri–Rolla, Rolla, MO 65401-0249, U.S.A.

**Abstract**—The problem of steady-state penetration by a semi-infinite, rigid cylindrical penetrator with an ellipsoidal nose into an infinite, rigid–viscoplastic target has been studied. The target material is assumed to obey a generalized form of Von Mises yield criterion to account for the strain-rate dependence. Contact between target and penetrator is assumed to be smooth. Computed results show that the deformation field adjacent to the nose of the penetrator is significantly different in the ellipsoidal case from what it is when the nose is hemispherical. Results presented graphically include the dependence of the axial resisting force on penetrator speed, the ratio of the major to minor axes of its ellipsoidal nose, and the strain-rate hardening parameter of the target. Also depicted are the normal pressure over the penetrator nose and the velocity field in different parts of the target.

## INTRODUCTION

In simple theories of penetration, the material properties of target and penetrator are often represented only by constant characteristic stresses, as for example in Tate [1]. Although this approach leads to results that are qualitatively correct, it can be difficult to use quantitatively. Some of the problems have to do with actual deformations in target and penetrator including lateral motion, and others are associated with the fact that the plastic flow stress is determined only by the deviatoric components of stress whereas the spherical or pressure component, which may be quite large ahead of the penetrator and contributes significantly to the retardation of the penetrator, is unrelated to flow stress (e.g. see Wright [2]). In developing an engineering model for penetration and perforation, Ravid and Bodner [3] assumed simple kinematics for the flow around the penetrator and then adjusted the unknown parameters by utilizing an upper bound theorem of plasticity modified to include dynamic effects.

In [4], Batra and Wright have presented a detailed numerical solution to the following idealized penetration problem. It was assumed that

(1) the rod is semi-infinite in length and that the target is infinite with a semi-infinite hole,
(2) the rate of penetration and all flow fields are steady as seen from the nose of the penetrator,
(3) no shear stress can be transmitted across the target–penetrator interface,
(4) the deforming material was taken to be rigid–perfectly plastic.

They studied the problem of the deforming target and a rigid penetrator having a circular cylindrical body and a hemispherical nose.

Batra and Wright's calculations revealed that strain rates in the target material that is ahead of the penetrator are of the order of $10^5$ sec$^{-1}$. Since many materials used in such applications have strain-rate sensitive properties, we extend herein the previous work to viscoplastic materials. Also, the penetrator nose is taken to be ellipsoidal. As in the previous work [4], the objective here is to study the idealized penetration problem in detail and possibly shed some light on the aforementioned factors. The problem studied herein simulates approximately the following situation: the penetrator is in the intermediate stages of penetration so that the active target–penetrator interface is at least one or two penetrator diameters away from either target face, and the remaining penetrator is still much longer than several diameters and is still traveling at a speed close to its striking velocity. For this case the first two assumptions stated in the second paragraph above are quite reasonable and are also made in this work. It should be emphasized that we have not incorporated any fracture or failure criterion in our work. Thus the material is presumed to undergo unlimited plastic deformations.

## FORMULATION OF THE PROBLEM

We presume that the deformations of the target appear to be independent of time to an observer situated on the penetrator nose and moving with it at a uniform velocity $v_0\mathbf{e}$, $\mathbf{e}$ being a unit vector along the direction of motion of the rigid penetrator. We use a cylindrical co-ordinate system attached to the center of the penetrator nose, with $z$-axis pointing into the target.

Equations governing the target deformations are:

$$\operatorname{div} \mathbf{v} = 0, \tag{1}$$

$$\rho(\mathbf{v} \cdot \operatorname{grad})\mathbf{v} = \operatorname{div} \boldsymbol{\sigma}. \tag{2}$$

Here $\mathbf{v}$ is the velocity of a target particle as seen by an observer situated on the penetrator, $\rho$ is the mass density and $\boldsymbol{\sigma}$ is the Cauchy stress tensor. Equation (1) implies that the deformations of the target are isochoric, and eqn (2) expresses the balance of linear momentum. We neglect the elastic deformations of the target and assume that its material obeys the following constitutive relation for $\boldsymbol{\sigma}$:

$$\boldsymbol{\sigma} = -p\mathbf{1} + 2\mu(I)\mathbf{D}, \qquad I \neq 0, \tag{3}$$

$$2\mu(I) = \sigma_0(1 + bI)^m/\sqrt{3}\,I, \tag{4}$$

$$\mathbf{D} = [\operatorname{grad} \mathbf{v} + (\operatorname{grad} \mathbf{v})^T]/2, \tag{5}$$

$$I^2 = \tfrac{1}{2} \operatorname{tr} \mathbf{D}^2. \tag{6}$$

In these equations, $p$ is the hydrostatic pressure that is not determined by the deformation history of the target, $\mathbf{D}$ is the stretching tensor, $\sigma_0$ is the yield stress in simple tension or compression, parameters $b$ and $m$ describe the strain-rate hardening of the material, and $\operatorname{tr}(\mathbf{D}^2)$ equals the sum of the diagonal terms of the square matrix $\mathbf{D}^2$. Equation (3) can also be viewed as a constitutive relation for an incompressible viscous fluid with viscosity coefficient equal to $\sigma_0(1 + bI)^m/(2\sqrt{3}\,I)$. Implicit in eqn (3) is the assumption that the Von Mises yield surface is given by

$$\operatorname{tr}(\mathbf{s}^2) = \tfrac{2}{3}\sigma_0^2(1 + bI)^{2m}, \tag{7}$$

$$\mathbf{s} = \boldsymbol{\sigma} + p\mathbf{1}. \tag{8}$$

The tensor $\mathbf{s}$ is the deviatoric stress tensor.

Ravid and Bodner [3] have used a constitutive relation similar to eqn (3) and assumed that

$$2\mu(I) = \sigma_0(1 + C \log_{10}(2I/\sqrt{3}))/\sqrt{3}\,I, \tag{9}$$

where $C$ is a material constant and is taken to be zero for strain rates lower than unity. The constitutive relation for a Bingham solid [5] results by taking $m = 1$ and interpreting $b$ properly. Zienkiewicz *et al.* [6] took

$$2\mu(I) = [\sigma_0 + (2I/\gamma\sqrt{3})^{1/n}]/\sqrt{3}\,I \tag{10}$$

and asserted that it corresponds to Perzyna's viscoplastic model. In eqn (10) $\gamma$ and $n$ are temperature-dependent material constants. Our choice [eqns (3, 4)] was motivated by the desire to generalize the power law model used by Burns [7] and Shawki *et al.* [8] so that it is also valid for quasistatic tests. This generalized constitutive model that also includes thermal softening and strain-hardening has been used by Wright and Batra [9], and Batra

[10] to study adiabatic shear bands. For the simple shearing stress state, a curve fit to Costin *et al.*'s [11] experimental data gives $b = 10^4$ and $m = 0.025$ for a hard steel.

Equation (1) and equations obtained by substitution of eqns (3)–(5) into eqn (2) are the field equations which together with suitable boundary conditions are to be solved for $p$ and $\mathbf{v}$. Before stating the boundary conditions, we non-dimensionalize the variables as follows:

$$\bar{\sigma} = \sigma/\sigma_0, \qquad \bar{\mathbf{s}} = \mathbf{s}/\sigma_0, \qquad \bar{p} = p/\sigma_0,$$

$$\bar{r} = r/r_0, \qquad \bar{z} = z/r_0, \qquad \bar{\mathbf{v}} = \mathbf{v}/v_0, \qquad \bar{b} = bv_0/r_0. \tag{11}$$

Here $(r, z)$ denote the co-ordinates of a point with respect to the cylindrical co-ordinate system chosen, and $r_0$ is the radius of the cylindrical body of the penetrator. The field equations written in terms of the non-dimensional variables are:

$$\operatorname{div} \mathbf{v} = 0 \tag{12}$$

$$-\operatorname{grad} p + \operatorname{div} \{\mu[(\operatorname{grad} \mathbf{v} + (\operatorname{grad} \mathbf{v})^{\mathrm{T}}]\} = \alpha(\mathbf{v} \cdot \operatorname{grad})\mathbf{v}, \tag{13}$$

where

$$\mu(I) = (1 + bI)^{m}/2\sqrt{3}\, I, \tag{14}$$

and

$$\alpha = \rho v_0^2/\sigma_0 \tag{15}$$

is a non-dimensional number. In writing eqns (12)–(14), we have dropped the superimposed bars and have used grad and div to denote the gradient and divergence operators in non-dimensional co-ordinates.

For the boundary condition on the penetrator–target interface, we assume that

$$\mathbf{t} \cdot (\sigma \mathbf{n}) = 0, \tag{16}$$

$$\mathbf{v} \cdot \mathbf{n} = 0, \tag{17}$$

where $\mathbf{n}$ and $\mathbf{t}$ are, respectively, a unit normal and a unit tangent vector on the interface. The boundary condition (16) represents smooth contact between the penetrator and target. This appears reaonable since a thin layer of material at the interface either melts or is severely degraded by adiabatic shear. The boundary condition (17) represents no interpenetration of the target material into the penetrator and vice versa. At points far away from the penetrator we require that

$$|\mathbf{v} + \mathbf{e}| \to 0 \quad \text{as} \quad (r^2 + z^2)^{1/2} \to \infty, \qquad z > -\infty, \tag{18}$$

$$|\sigma \mathbf{n}| \to 0 \quad \text{as} \quad z \to -\infty, \qquad r \geqslant r_0, \tag{19}$$

where $\mathbf{e}$ is a unit vector along the positive $z$-axis, as before. That is, the target material ahead of the penetrator nose and far away from it appears to approach the penetrator with a uniform velocity and the one behind the nose but very far from it is virtually traction free.

Note that the field eqns (13) are nonlinear in $\mathbf{v}$. A solution of eqns (12) and (13) under the boundary conditions (16)–(19), if there exists one, will depend upon the rate at which quantities in (18) and (19) decay to zero. Even for the prescribed rate of decay, the solution may not be unique. We will gloss over these rather difficult questions and seek an approximate solution of these equations numerically. The hope is that the numerical solution is meaningful for the physical problem at hand.

## FINITE ELEMENT FORMULATION OF THE PROBLEM

We replace the infinite target region by the bounded region R shown in Fig. 1 and the boundary conditions (18) and (19) by

$$\sigma_{zz} = 0, \quad v_r = 0 \qquad \text{on the surface AB,}$$
$$\sigma_{rz} = 0, \quad v_r = 0 \qquad \text{on the axis of symmetry DE,}$$
$$v_r = 0, \quad v_z = -1.0 \qquad \text{on the bounding surface EFA.} \tag{20}$$

That the region considered is adequate is justified by the computed results presented below which show that noticeable deformations of the target occur only in the region surrounding the penetrator and at target particles whose distance form the penetrator is at most $2r_0$.

Referring the reader to [12] for details, we simply note that a weak formulation of the problem defined by eqns (12), (13), (16), (17) and (20) is that equations

$$\int_R \psi(\operatorname{div} \mathbf{v})\, dv = 0, \tag{21}$$

$$\int_R p(\operatorname{div} \boldsymbol{\phi})\, dv - \int_R \mu(I)\{\mathbf{D}:[\operatorname{grad} \boldsymbol{\phi} + \operatorname{grad} \boldsymbol{\phi})^T]\}\, dv = \alpha \int_R [(\mathbf{v}\cdot\operatorname{grad})\mathbf{v}]\cdot\boldsymbol{\phi}\, dv \tag{22}$$

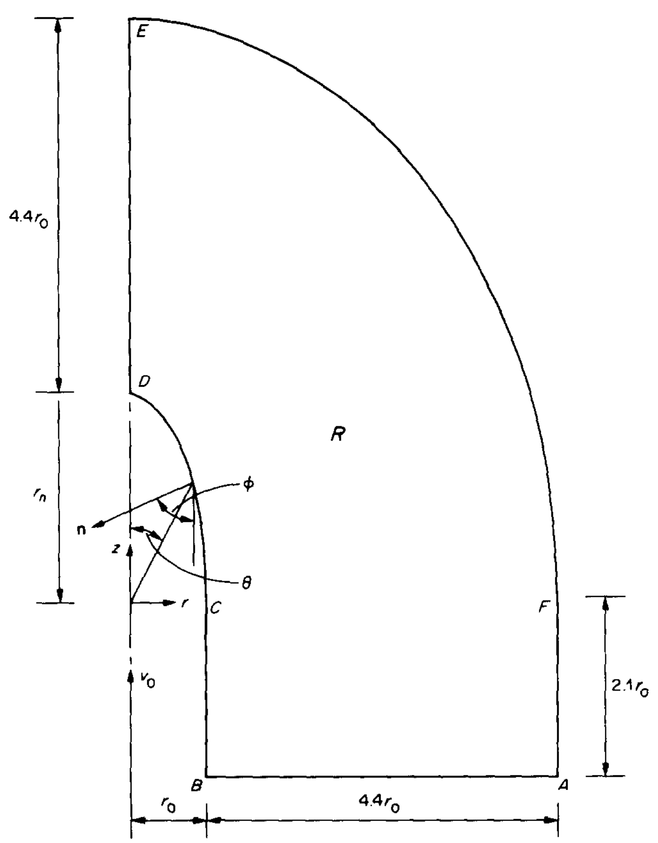


Fig. 1. The region modeled.

hold for every smooth functions $\psi$ and $\boldsymbol{\phi}$ defined on $R$ such that $\phi_r = 0$ on AB and DE; $\boldsymbol{\phi} = \mathbf{0}$ on EFA and $\boldsymbol{\phi}\cdot\mathbf{n} = 0$ on the target–penetrator interface BCD. Since eqns (21) and (22) are nonlinear in $\mathbf{v}$, the following iterative technique has been employed:

$$\int_R \psi(\operatorname{div}\mathbf{v}^i)\,\mathrm{d}v = 0, \tag{23}$$

$$\int_R p^i(\operatorname{div}\boldsymbol{\phi})\,\mathrm{d}v - \int_R \mu(I^{i-1})\{\mathbf{D}^i:[\operatorname{grad}\boldsymbol{\phi} + (\operatorname{grad}\boldsymbol{\phi})^{\mathrm{T}}]\}\,\mathrm{d}v = \alpha\int_R [(\mathbf{v}^{i-1}\cdot\operatorname{grad})\mathbf{v}^i]\cdot\boldsymbol{\phi}\,\mathrm{d}v, \tag{24}$$

where $i$ is the iteration number. The solution was taken to have converged, if at each nodal point,

$$|\mathbf{v}^i - \mathbf{v}^{i-1}| \leqslant 0.01\,|\mathbf{v}^{i-1}|,$$

where

$$|\mathbf{v}|^2 = v_r^2 + v_z^2.$$

## COMPUTATION AND DISCUSSION OF RESULTS

The finite element code developed earlier [4] to solve the problem when the target material is modeled as rigid–perfectly plastic and the penetrator nose is hemispherical has been modified to solve the present problem. It employs six-noded isoparametric triangular elements with $v_r$ and $v_z$ approximated by quadratic functions over an element and $p$ by a linear function defined in terms of its values at the vertices of the triangular element. The accuracy of the code was established by solving a simple problem for an incompressible Navier–Stokes fluid.

The computational procedure was started by taking $\mathbf{v}^0 = \mathbf{0}$, $\mu(I^0) = 10^4$. It took 19 iterations for the solution to converge when $\alpha = 2$ and the nose is hemispherical. The number of iterations required to obtain the solution decreased with an increase in the ratio $r_n/r_0$ when $\alpha = 2$. However, for $r_n/r_0 = 1$, the number of iterations increased with $\alpha$, but for $r_n/r_0 = 2$ it decreased with an increase in $\alpha$. Numerical experiments with different grids were conducted first by increasing the number of elements used and then by varying their size but keeping the number of elements used constant. The grid with 8 rows of elements in the axial direction, 8 uniformly spaced rows of elements in the circumferential direction and 8 rows behind the plane $z = 0$, was found to be optimum in the sense that the change in the normal stress at the penetrator nose tip was less than 0.1% with further refinements of the grid. The grid used had a pattern similar to that employed in [4]. The dividing surfaces between elements intersected the $z$-axis at points distant 0.475, 0.969, 1.483, 2.017, 2.573, 3.151, 3.752, 4.377 from the nose tip. The $z$-co-ordinate of the horizontal surfaces between rows of elements behind the $z = 0$ plane were $-0.156$, $-0.335$, $-0.540$, $-0.773$, $-1.041$, $-1.347$, $-1.697$, $-2.09$. For $\alpha = 2.0$, $r_n/r_0 = 2.0$, $m = 0.0$, and $b = 0.0$, the total axial force, defined below by eqn (29), obtained by using 4, 6, 7, 12 and 13 quadrature points was computed to be 2.6117, 2.6479, 2.6524, 2.6714 and 2.6720 respectively. The results presented below have been obtained by using 4 quadrature points.

Figure 2 depicts the velocity of the target particles for $\alpha = 4$ and $r_n/r_0 = 2.0$ as seen by an observer sitting on the penetrator nose. It is apparent that significant deformations of the target occur at points within $2r_0$ of the penetrator boundaries. The velocity fields for other cases studied have a similar pattern. At target points that lie to the rear of the center of the penetrator nose, the flow quickly becomes parallel to the axis of the penetrator. In Fig. 3 is shown the non-dimensional normal stress on the penetrator nose for different choices of various parameters. Values of parameters for various curves in this and subsequent figures, unless specified otherwise, are identified in Table 1. The change in nose shape from hemispherical to ellipsoidal reverses the curvature of the normal stress vs $\theta$

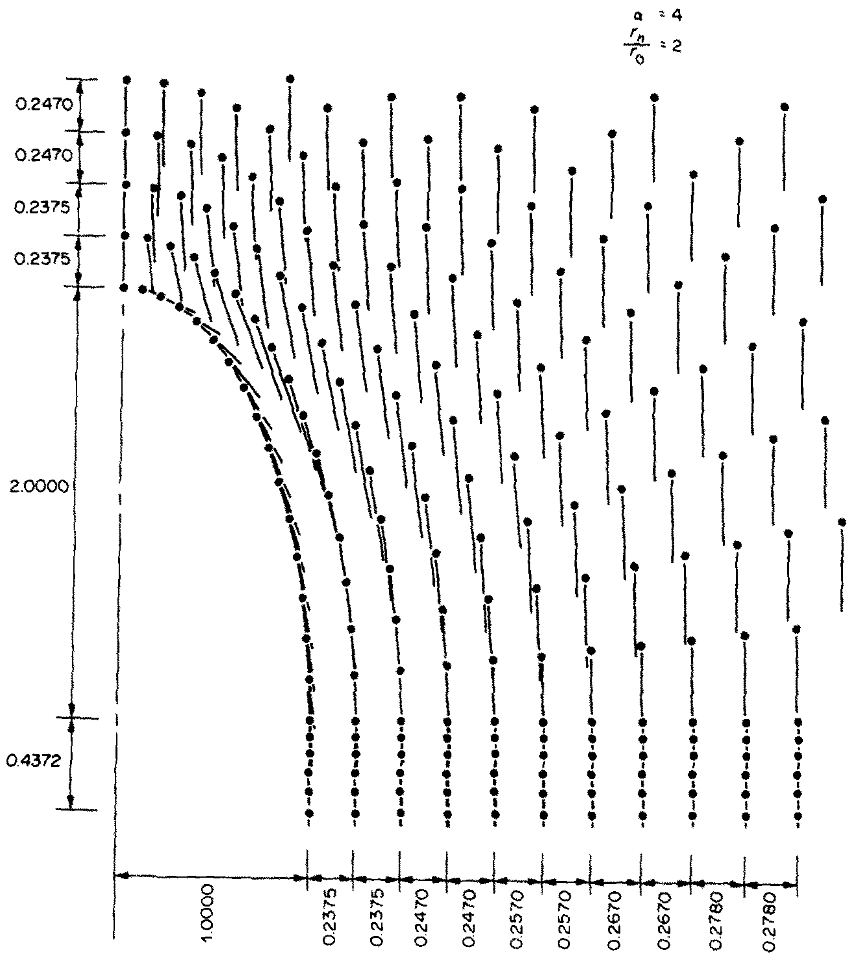


Fig. 2. Typical velocity field.

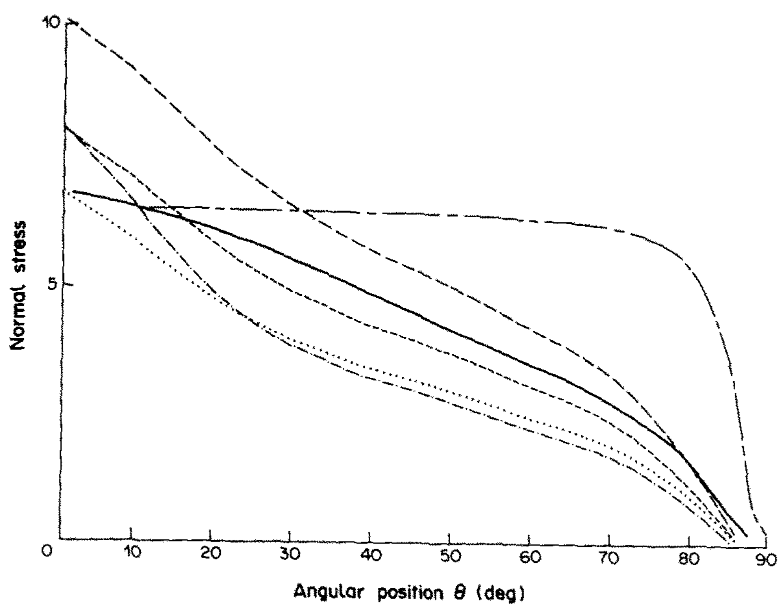


Fig. 3. Normal stress distribution on the penetrator nose.

Table 1. Legend for figures

| Curve type | Parameter values |
|---|---|
| — — — — — — — | $\frac{r_n}{r_0} = 2.0,\ b = 10^8,\ m = 0.03,\ \alpha = 2.0$ |
| - - - - - - - - - | $\frac{r_n}{r_0} = 2.0,\ b = 10^4,\ m = 0.03,\ \alpha = 2.0$ |
| ..................... | $\frac{r_n}{r_0} = 2.0,\ b = 0,\ m = 0,\ \alpha = 2.0$ |
| — — — — — — | $\frac{r_n}{r_0} = 2.0,\ b = 0,\ m = 0,\ \alpha = 4.0$ |
| ———————— | $\frac{r_n}{r_0} = 1.0,\ b = 0,\ m = 0,\ \alpha = 2.0$ |
| ————————— | $\frac{r_n}{r_0} = 0.2,\ b = 0,\ m = 0,\ \alpha = 2.0$ |

curve from convex downwards to concave downwards. This change was observed even for $r_n/r_0 = 1.1$. For $\alpha = 2$, the normal stress at the nose tip was essentially unchanged for $0.2 \leqslant r_n/r_0 \leqslant 2.4$. For $r_n/r_0 = 0.2$, the nose shape is essentially flat and, as expected, the normal stress on it stays uniform and drops off rapidly near the periphery. The increase in $\alpha$, $m$ or $b$ increases the normal stress on the penetrator nose.

The non-dimensional axial resisting force experienced by the penetrator as various

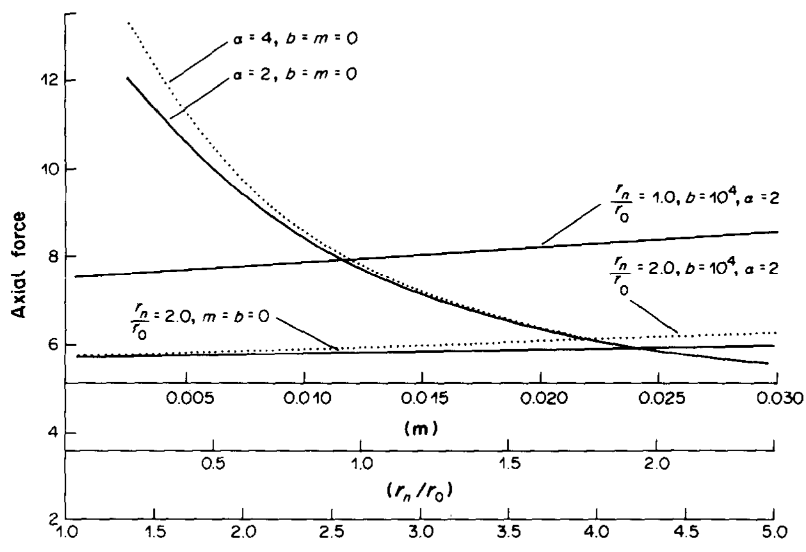

Fig. 4. Dependence of axial force on various factors.

parameters are changed is plotted in Fig. 4. Equations obtained by fitting curves to the computed data are:

$$F = 2.58(1 + 0.00738\alpha - 0.000569\alpha^2), \quad 1 \leqslant \alpha \leqslant 5, \quad \frac{r_n}{r_0} = 2.0, \quad b = m = 0, \tag{25}$$

$$F = 2.611(1 + 6.761m + 20.465m^2), \quad 0 \leqslant m \leqslant 0.03, \quad \frac{r_n}{r_0} = 2.0, \quad b = 10^4, \quad \alpha = 2.0, \tag{26}$$

$$F = 4.456(1 + 7.28m + 23.478m^2), \quad 0 \leqslant m \leqslant 0.03, \quad \frac{r_n}{r_0} = 1.0, \quad b = 10^4, \quad \alpha = 2.0, \tag{27}$$

$$F = 13.041\left[1.0 - 1.3086\frac{r_n}{r_0} + 0.9504\left(\frac{r_n}{r_0}\right)^2 - 0.3432\left(\frac{r_n}{r_0}\right)^3 + 0.0477\left(\frac{r_n}{r_0}\right)^4\right],$$

$$0.2 \leqslant \frac{r_n}{r_0} \leqslant 2.4, \quad b = m = 0, \quad \alpha = 4 \tag{28}$$

$$F = 10.857\left[1.0 - 1.0455\frac{r_n}{r_0} + 0.6294\left(\frac{r_n}{r_0}\right)^2 - 0.1975\left(\frac{r_n}{r_0}\right)^3 + 0.0246\left(\frac{r_n}{r_0}\right)^4\right],$$

$$0.2 \leqslant \frac{r_n}{r_0} \leqslant 2.4, \quad b = m = 0, \quad \alpha = 2,$$

where

$$F = 2\int_0^{\pi/2} (\mathbf{n}\cdot\boldsymbol{\sigma}\mathbf{n})\sin\theta\cos\phi\left[\sin^2\theta + \left(\frac{r_n}{r_0}\right)^2\cos^2\theta\right]^{1/2} d\theta, \tag{29}$$

$\phi$ is the angle which the unit normal to the nose makes with the penetrator axis as shown in Fig. 1. The corresponding axial force in physical units is given by $F(\pi r_0^2\sigma_0)$. It is clear from these results that changing the nose shape from hemispherical to ellipsoidal with $r_n/r_0 = 2.0$ reduces the axial resisting force to one-half of its value. For a fixed $r_n/r_0$ and $m$, the axial force depends rather weakly upon $\alpha$. This weak dependence of $F$ upon $\alpha$ is perhaps one reason why the choice of constant target resistance in simple theory of Tate [1] gives good qualitative results. Even though the coefficient of $m^2$ in eqns (25) and (26) is nearly 3 times that of $m$, the dependence of the axial force $F$ upon the strain-rate hardening coefficient $m$ is essentially linear. It is so because the values of $m$ for typical steels are much smaller than one. This linear dependence of $F$ upon $m$ becomes transparent from the plots of Fig. 4.

Computed results indicate that for $1 \leqslant \alpha \leqslant 5$, $r_n/r_0 = 2.0$, $b = m = 0$, the hydrostatic pressure at the nose tip increases essentially linearly from 5.6 to 8.2 and the normal compressive stress from 6.22 to 8.84. It is apparent that the hydrostatic pressure contributes significantly to the values of $\sigma_{rr}$ and $\sigma_{zz}$. Figure 5 shows that the principal stress component $-\sigma_{zz}$ along the axis in front of the penetrator falls off rapidly with the distance. The stresses at points situated more than $3r_0$ from the nose tip cannot be accurately determined since the velocity gradients there are extremely small. The values of $\sigma_{zz}$ at points on the centerline which are at a distance of $3r_0$ and more from the nose tip equal essentially the hydrostatic pressure.

In Fig. 5 is also plotted the variation of the strain-rate measure $I$ along the axial line. These nondimensional values need to be multiplied by $v_0/r_0$, which typically equals $10^5$, to arrive at the corresponding dimensional effective strain-rate measure $I$. Thus strain-rates of the order of $2 \times 10^5\,\text{sec}^{-1}$ occur at points in the vicinity of the penetrator nose. On the axial line, peak values of $I$ are higher near the nose tip for $r_n/r_0 = 2.0$ as compared with those for lower values of $r_n/r_0$. However, near the periphery of the penetrator nose and its cylindrical body, the strain-rate measure $I$ for the blunt nose increases by an order of magnitude whereas that for the ellipsoidal and hemispherical nose, it drops by a factor of 10. This is shown in Fig. 6 wherein is also plotted the nondimensional velocity, tangential to the penetrator nose, for different values of various parameters. Again the nose shape is the major influencing factor. However, $v_z$ at points on the centerline ahead of the penetrator nose is not affected that much by the nose shape except for $r_n/r_0 = 0.2$. The decay rate of $|v_z + \mathbf{e}|$ for $1 \leqslant \frac{r_n}{r_0} \leqslant 2.4$ is nearly constant but is appreciably less for $r_n/r_0 = 0.2$. The nose shape does change rather noticeably the relative $z$-velocity of points on the lines $z = 0$ and $z = 2.09$. This follows from the results depicted in Figs 7 and 8 which also show that more of the target material at the sides of the penetrator deforms for a penetrator with an ellipsoidal nose, even though it is not true ahead of the penetrator, as noted earlier. Two of the curves in these figures essentially overlap.

We note that the target material within some distance inside the boundary EFA does not deform at all and the deformations are essentially independent of $z$ near the boundary

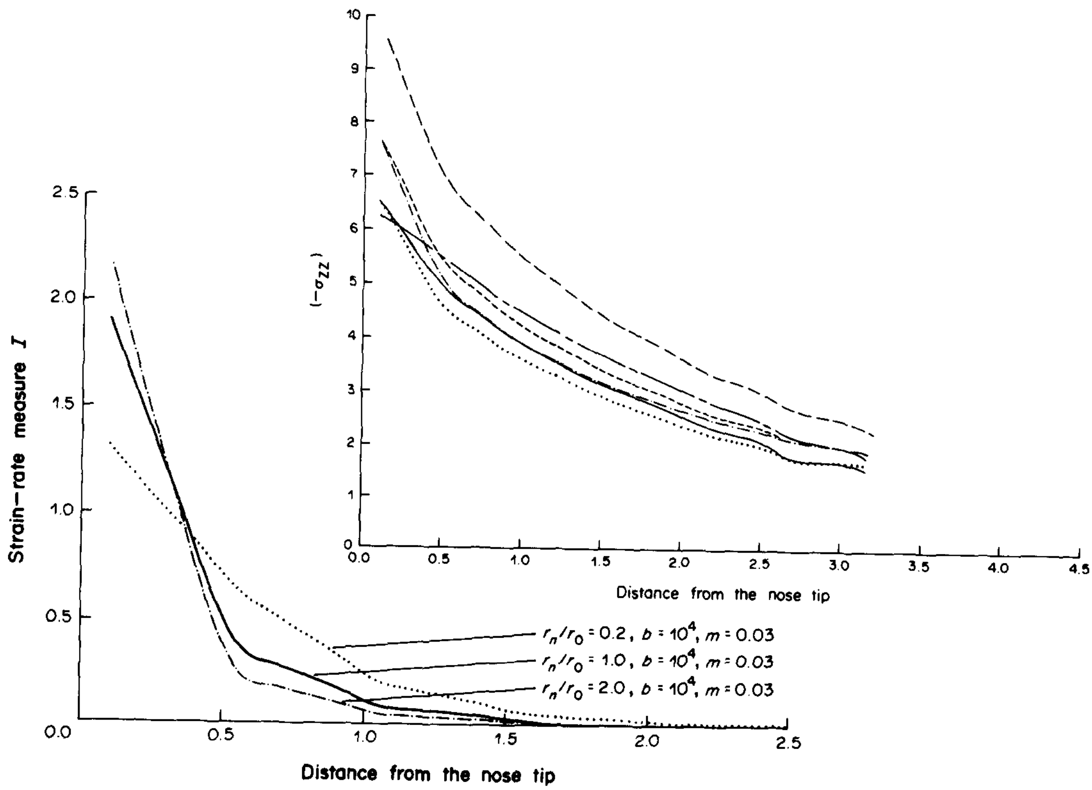


Fig. 5. Variation of $-\sigma_{zz}$ and strain-rate measure $I$ on the centerline with distance from the nose tip.

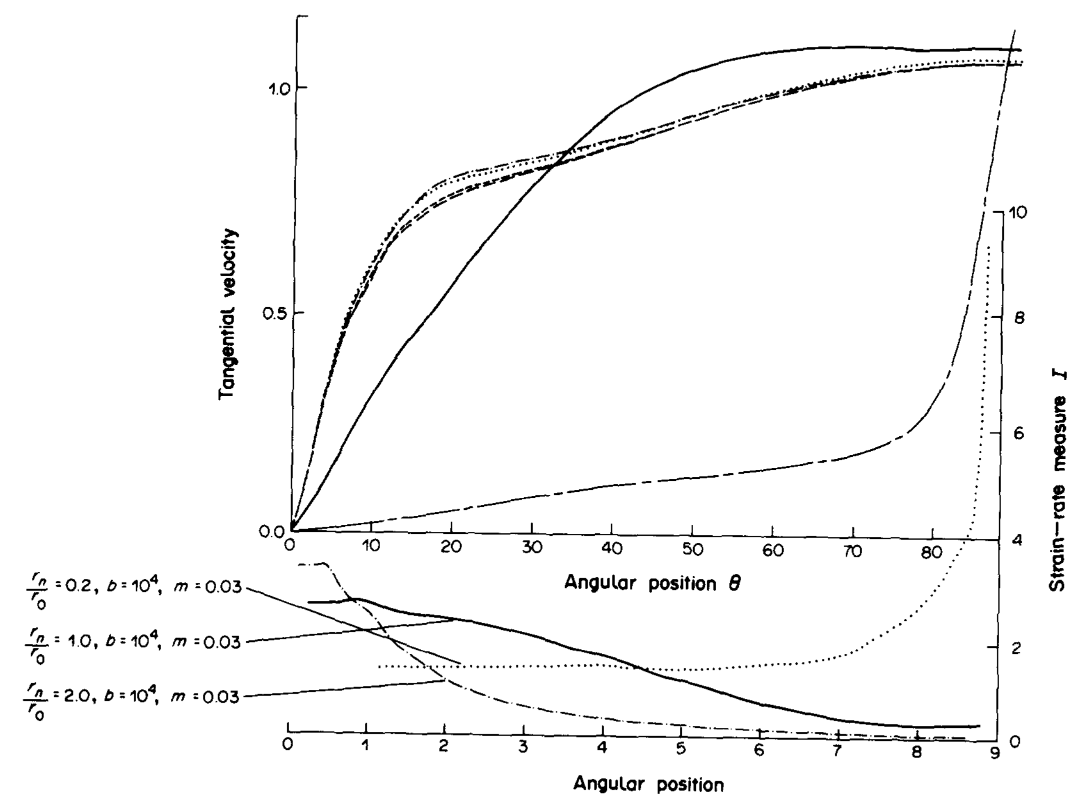


Fig. 6. Variation of tangential velocity and strain-rate measure on the penetrator nose.

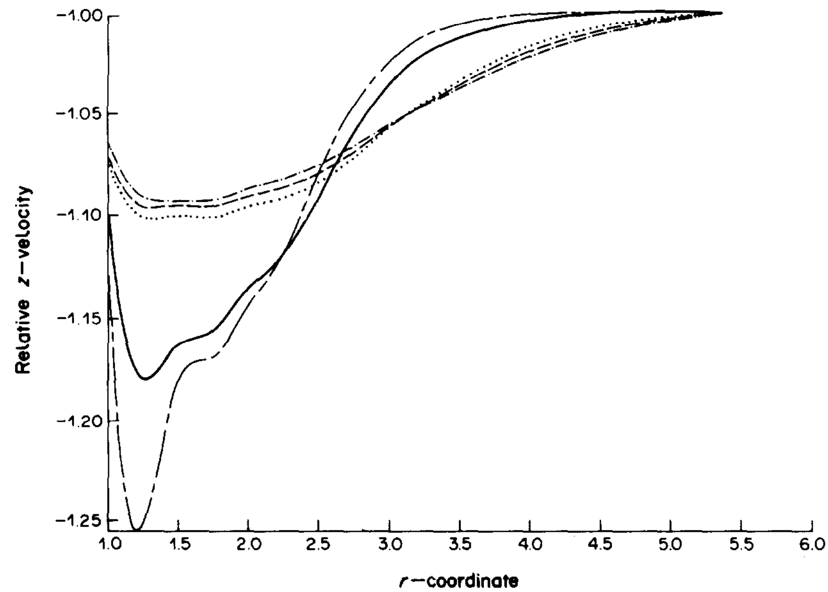


Fig. 7. Variation of relative $z$-velocity with radial co-ordinate $r$ on the line $z = 0$.

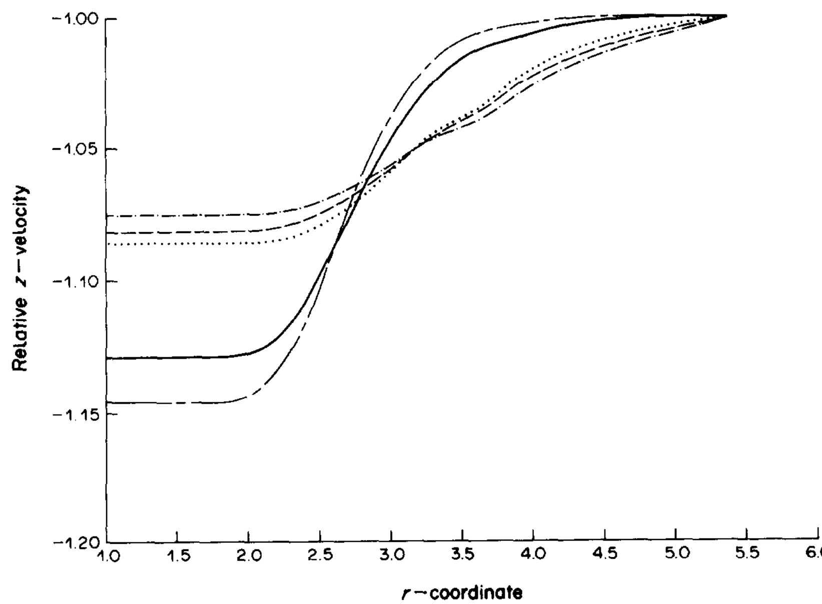


Fig. 8. Variation of relative $z$-velocity with radial co-ordinate $r$ on the line $z = -2.09$.

AB. It is therefore reasonable to conclude that the target region chosen for computation is sufficient to obtain a good description of the deformations in the vicinity of the penetrator nose.

## CONCLUSIONS

For the range of values of $r_n/r_0$, $\alpha$ and $m$ studied, the ratio $r_n/r_0$ of the radius of the nose to that of the cylindrical body of the penetrator has the most effect on the axial resisting force experienced by the penetrator. The retardation force depends rather weakly on $\alpha$ and $m$. In all cases, significant target deformations occur only within $2r_0$ of the penetrator. Whereas for $r_n/r_0 = 1.0$, the target material adjacent to the sides of the penetrator appears to extrude rearwards in a uniform block that is separated from the bulk of the target material by a narrow region with a sharp velocity gradient, such is not the case for $r_n/r_0 = 2.0$. In the latter case there is no noticeable region of steep velocity gradients.

For $\alpha = 5$ and $r_n/r_0 = 2.0$ the target material seemed to separate from the sides of the penetrator nose. This provides a limiting value for the validity of our calculations since flow separation has not been built into our model. Maximum normal stress and the maximum hydrostatic pressure occur at the nose tip, and fall off rapidly away from that point. These peak values depend significantly upon $\alpha$.

We hope that results presented here will prove useful in devising or checking the results from simpler engineering theories of penetration.

*Acknowledgements*—This work was supported by the U.S. Army Research Office contract DAAG29-85-K-0238 to the University of Missouri-Rolla. I thank Pei-Rong Lin for his help in plotting Fig. 2.

## REFERENCES

[1] A. TATE, *J. Mech. Phys. Solids* **15**, 387 (1967); *ibid.* **17**, 141 (1969).
[2] T. W. WRIGHT, A survey of penetration mechanics for long rods. *Lecture Notes in Engineering. Vol. 3, Computational Aspects of Penetration Mechanics* (Edited by J. Chandra and J. Flaherty). Springer-Verlag, New York (1983).
[3] M. RAVID and S. R. BODNER, *Int. J. Engng Sci.* **21**, 577 (1983).
[4] R. C. BATRA and T. W. WRIGHT, *Int. J. Engng Sci.* **24**, 41 (1986).
[5] N. CRISTESCU and I. SULICIU, *Viscoplasticity.* Martinus Nijhoff, The Hague (1982).
[6] O. C. ZIENKIEWICZ, E. ONATE and J. C. HEINRICH, *Int. J. numer. Meths Engng* **17**, 1497 (1981).
[7] T. J. BURNS, Sandia Rep. SAND83-1907. Sandia National Laboratories, Albuquerque, NM (1983).
[8] T. G. SHAWKI, R. J. CLIFTON and G. MAJDA, Brown University Rep. ARO DAAG 29-81-K-0121/3, Providence, RI (1983).
[9] T. W. WRIGHT and R. C. BATRA, *Proc. IUTAM Symp. Macro- and Micro-Mechanics of High Velocity Deformation and Fracture.* Springer-Verlag, New York–Berlin (1986).
[10] R. C. BATRA, *Int. J. Plast.* **3**, 75 (1987).
[11] L. S. COSTIN, E. E. CRISMAN, R. H. HAWLEY and J. DUFFY, *Inst. Phys. Conf. Ser. no.* **47**, 90 (1979).
[12] E. BECKER, G. CAREY and J. T. ODEN, *Finite Element—An Introduction*, Vol. 1, Prentice-Hall, Englewood Cliffs, NJ (1981).

(*Received* 23 *December* 1986)